Available online at www.sciencedirect.com
SCIENCE DIRECT
Journal of Asian Earth Sciences 26 (2006) 105–120
Journal of Asian Earth Sciences
www.elsevier.com/locate/jaes

Carbonatite-like dykes from the eastern Himalayan syntaxis: geochemical, isotopic, and petrogenetic evidence for melting of metasedimentary carbonate rocks within the orogenic crust

Yan Liu[a,*], Zsolt Berner[b], Hans-Joachim Massonne[c], Dalai Zhong[d]

[a]*Institute of Geology, Chinese Academy of Geological Sciences, Beijing 100037, People's Republic of China*
[b]*Institut für Mineralogie und Geochemie, Universität Karlsruhe, Kaiserstraße 12, D-76128 Karlsruhe, Germany*
[c]*Institut für Mineralogie und Kristallchemie, Universität Stuttgart, Azenbergstr. 18, D-70174 Stuttgart, Germany*
[d]*Institute of Geology and Geophysics, Chinese Academy of Sciences, Beijing 100029, People's Republic of China*

Received 9 April 2004; revised 27 August 2004; accepted 22 October 2004

Abstract

Within the eastern Himalayan syntaxis, carbonatite-like dykes occur in granulite facies gneisses of the Greater Himalayan Crystallines. Most dykes are dolomitic and are associated with scapolite-bearing hornblendite and glimmerite, which are separated from the country rocks by a selvage of altered rocks containing minerals such as diopside, tremolite, K-feldspar, albite, and calcite. Only a few dykes are calcitic with alteration halos containing wollastonite, calcite, anorthite, diopside, and scapolite. Dolomitic dykes as wide as several tens of metres contain irregular xenoliths of granulitic gneiss.

Geochemically, the carbonatite-like dykes differ significantly from mantle-derived carbonatites. The dyke rocks are poor in REEs, Ba, Sr, U, Th, Nb, F and P. Their $^{87}Sr/^{86}Sr$, $^{143}Nd/^{144}Nd$, $\delta^{18}O$ (relative to V-SMOW) and $\delta^{13}C$ (relative to V-PDB) values range from 0.709 to 0.712, 0.5117 to 0.5121, +8 to +24.4‰, and +0.80 to +3.55‰, respectively. These values are similar to those for most sedimentary carbonates suggesting that the carbonatite-like dykes were formed as melts from sedimentary carbonates at crustal levels. Structural analysis has shown that the Greater Himalayan Crystallines were extruded from beneath southern Tibet via ductile channel flow to overlie the limestone/marble-bearing Lesser Himalayan Crystallines. Fluxing of limestones below the Greater Himalayan Crystallines was probably triggered by the overlying Greater Himalayan Crystallines. K–Ar and Ar–Ar geochronology data obtained on amphibole and mica from the carbonate dykes indicate this event occurred during the late Neogene.

Keywords: Carbonatite; Dykes; Eastern Himalayan syntaxis; Sr isotopes; Nd isotopes; Stable isotopes; Trace element characteristics; Stable isotopes; Carbonate.

1. Introduction

The petrogenesis of carbonatite magmas has been controversially discussed since an igneous origin for such carbonate rocks was first proposed. It has been widely accepted since the mid-sixties that carbonatite magmas are ultimately derived from the Earth's mantle largely because they are enriched especially in F, P, Sr, Nb, REEs, U and Th, and their stable and radiogenic isotope signatures are unlike those of sedimentary limestones (Wyllie et al., 1990; Lentz, 1998, 1999). Thus, previous theories of carbonatite genesis related to the melting of sedimentary limestones were widely abandoned, although melting of this rock type is, in principle, possible as also shown by experimental studies (Wyllie and Tuttle, 1960; Fanelli et al., 1986; Lentz, 1998, 1999). Many petrologists consider carbonatites as secondary magmas derived at relatively low pressures through liquid immiscibility from parental silicate magmas of nephelinitic affinity (e.g. Le Bas, 1987; Kjarsgaard and Hamilton, 1988; Simonetti and Bell, 1994), whereas, others believe the existence of primary carbonatitic magmas originating in the mantle (e.g. Bailey, 1989; Harmer et al., 1998; Achterbergh

* Corresponding author.
E-mail address: yanliu0315@yahoo.com.cn (Y. Liu).

1367-9120/$ - see front matter © 2004 Elsevier Ltd. All rights reserved.
doi:10.1016/j.jseaes.2004.10.003

et al., 2002). Recently, the argument has been brought up that recycling of sedimentary carbon via subduction of the oceanic crust into the mantle is necessary to sustain carbonatite magmatism (Barker, 1996; Achterbergh et al., 2002; Hoernle et al., 2002). Others have argued for the origin of carbonate melts by deep mantle-plumes (Bell and Tilton, 2002). The above kinds of petrogenesis of igneous carbonate rocks are exclusive because no other possibilities seem to exist. For some carbonate-rich rocks, however, it is not known yet if they primarily have formed either as igneous or sedimentary rocks (e.g. Krishnamurthy et al., 2000; Le Bas et al., 2002). Here we present an example of unusual carbonate intrusive rocks appearing as dykes in granulite facies complex. Geochemical and isotopic data that relate to the origin of these dykes were reported and petrogenetic constraints were discussed.

2. Geological setting

2.1. General aspects

The eastern Himalayan syntaxis is located in the range of the two large peaks named Namche Barwa in the south and Giala Peri in the north of the eastern end of the Himalayas. The Yarlung Zangbo River passes through them forming a greater canyon (Fig. 1). Before the middle of the nineties, the eastern Himalayan syntaxis was one of the least-known segments of the Himalayas, partially because it is a remote and rugged terrain. According to studies several years ago, the eastern Himalayan syntaxis consists of three tectonic units: Gangdise, Yarlung Zangbo, and Himalayan units (Liu and Zhong, 1997, 1998; Burg et al., 1998). The Gangdise unit, a southern part of the Lhasa block, consists of granitoids, migmatites and amphibolite facies rocks, commonly covered by Palaeozoic and Mesozoic sediments. This unit, generally regarded as the eastern continuation of the Gangdise Batholith (Liu and Zhong, 1997, 1998; Burg et al., 1998), is separated from the Himalayan unit by the Yarlung Zangbo unit consisting of a mylonitic zone with lenses of metabasite and serpentinite. The basic-ultrabasic lenses of the Yarlung Zangbo unit suggest that the boundary between the Gangdise and the Himalayan units is an eastern extension of the Indus—Yarlung Zangbo suture between the Indian and Asian plates, which was folded around the eastern Himalayan syntaxis (Liu and Zhong, 1997, 1998; Burg et al., 1998). Recent detailed field mapping has revealed that the Himalayan unit is made up of the North Col greenschist to amphibolite facies complex, the Greater Himalayan Crystallines, the upper Lesser Himalayan Crystallines, and the lower Lesser Himalayan Crystallines from north to south (Fig. 1a and b). The North Col Formation, which was named by Yin and Guo (1978), occurs to the north of the Greater Himalayan Crystallines within the Mt. Qomolangma area, central Himalayas. The typical mineral assemblage in metapelites from the North Col complex consists of plagioclase + quartz + biotite + chlorite + epidote ± muscovite. Mineral assemblages of scapolite + actinolite + oligoclase, garnet + biotite + muscovite + oligoclase and sillimanite + cordierite + biotite occur in rocks at the bottom of this complex (Liu et al., 1990; Pognante and Benna, 1993; Lombardo and Rolfo, 2000; Searle et al., 2003). Within the eastern Himalayan syntaxis, the dominant mineral assemblage of the greenschist to amphibolite facies complex occurring to the north of the Greater Himalayan Crystallines is also plagioclase + quartz + biotite + chlorite + epidote ± muscovite. Thus, the greenschist to amphibolite facies complex of the eastern Himalayan syntaxis is also regarded as the North Col Formation. However, the mineral assemblage of staurolite + kyanite + K-feldspar + muscovite + quartz + epidote ± garnet occurs in metapelites at the bottom of the complex, different to that occurring at the bottom of the North Col Formation at the central Himalayas. A ductile normal fault, referred here to the south Tibet Detachment One (STD1), separates the North Col Formation from the Greater Himalayan Crystallines below (Fig. 1a and b). Strongly deformed granites occur along the contact between the North Col Formation and the Greater Himalayan Crystallines (Fig. 1a and b). Rocks of the Greater Himalayan Crystallines at the eastern Himalayan syntaxis are marked by the assemblages garnet + prismatic sillimanite + K-feldspar + antiperthite or plagioclase. Spinel + albite + biotite or spinel + cordierite ± orthopyroxene forms retrograde coronas around sillimanite and garnet. The prismatic sillimanite had been argued to replace early kyanite under higher temperature conditions, indicating that the Greater Himalayan Crystallines experienced high-pressure metamorphism (Liu and Zhong, 1997). The Greater Himalayan Crystallines were thrust southwards or southeastwards over the upper Lesser Himalayan Crystallines consisting generally of amphibolitic gneisses, sillimanite gneisses, granitic gneisses, and marble in the footwall by a ductile thrust system, which is referred to the Main Central Thrust One (MCT1) here (Fig. 1a and b). Further south, another ductile thrust system, named Main Central Thrust Two (MCT2) here, separates the upper Lesser Himalayan Crystallines above from the lower Lesser Himalayan Crystallines consisting generally of quartzite, calc-silicate schist, limestone, metapsammite and muscovite phyllite in the footwall (Fig. 1a and b). The recent field mapping of the eastern Himalayan syntaxis has, therefore, supported the current model proposed by Beaumont et al. (2001) and Grujic et al. (1996, 2002) that the hot Greater Himalayan Crystallines were also exhumed from beneath south Tibet to overlie the limestone/marble-bearing Lesser Himalayan Crystallines via ductile channel flow between the MCT1 and the STD1 faults (Fig. 1a and b).

2.2. Occurrences of carbonate-rich dykes

A distinctive feature between the Giala Peri and Namche Barwa peaks is the occurrence of numerous dykes with various compositions and different ages along the foliation

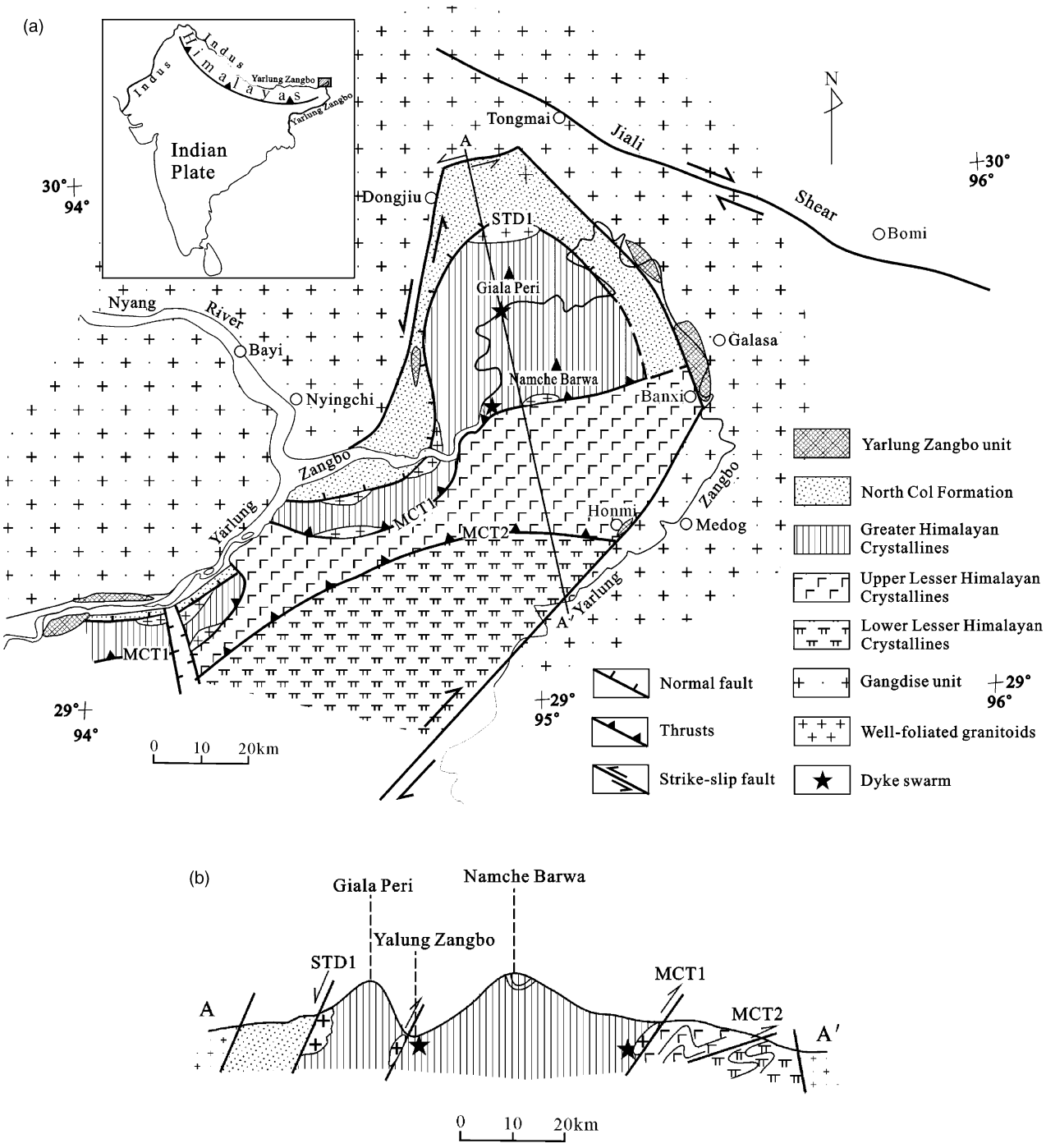

Fig. 1. (a) Geological sketch map of the eastern Himalayan syntaxis, after Liu and Zhong (1997) and Burg et al. (1998) and our own observations. Inlet is a large-scale location map. (b) Geological section, for locations see (a).

of the granulite facies gneisses of the Greater Himalayan Crystallines. Three rock types in the dyke swarms can be distinguished. One type is characterized by carbonate rocks forming two large dyke swarms within the eastern Himalayan syntaxis (Fig. 1a and b). The larger swarm of carbonate dykes occurs between the Namche-Barwa and Giala Peri peaks, and consists of several hundreds of dykes. The smaller dyke swarm is located along the MCT1 fault (Fig. 1a and b), and consists of several tens of dykes. Individual carbonate dykes vary from a few centimetres to several tens of metres in width. They can be up to several kilometres long, commonly appearing as foliated-banded sheet-like bodies. Most carbonate dykes are dolomitic. Only a few are calcitic. All of the carbonate dykes have fine-grained dark 'chilled' margins from several millimeters to centimeters in thickness and extensive metasomatic

alteration halos. Large dolomitic bodies commonly contain xenoliths of granulitic gneiss with irregular shape. These xenoliths can be distinguished from the host rocks by a light-color alteration (Fig. 2a). Cross-cutting relationships of the carbonate-rich dykes were observed in the field (Fig. 2b). From centre to margin of the dykes, the size of the mineral grains decreases (Fig. 2c). These field characteristics, differing significantly from ordinary carbonate dykes of hydrothermal origin, are similar to those of typically igneous dykes including mantle-derived carbonatites documented in numerous publications (e.g. Tuttle and Gittins, 1966; Le Bas, 1981). Thus, the above field observations indicate clearly an igneous origin of the carbonate-rich dykes from the eastern Himalayan syntaxis. The dolomitic dykes are commonly associated or interlayered with scapolite hornblendite, whereas no typically associated silicate rocks occur around the calcitic dykes.

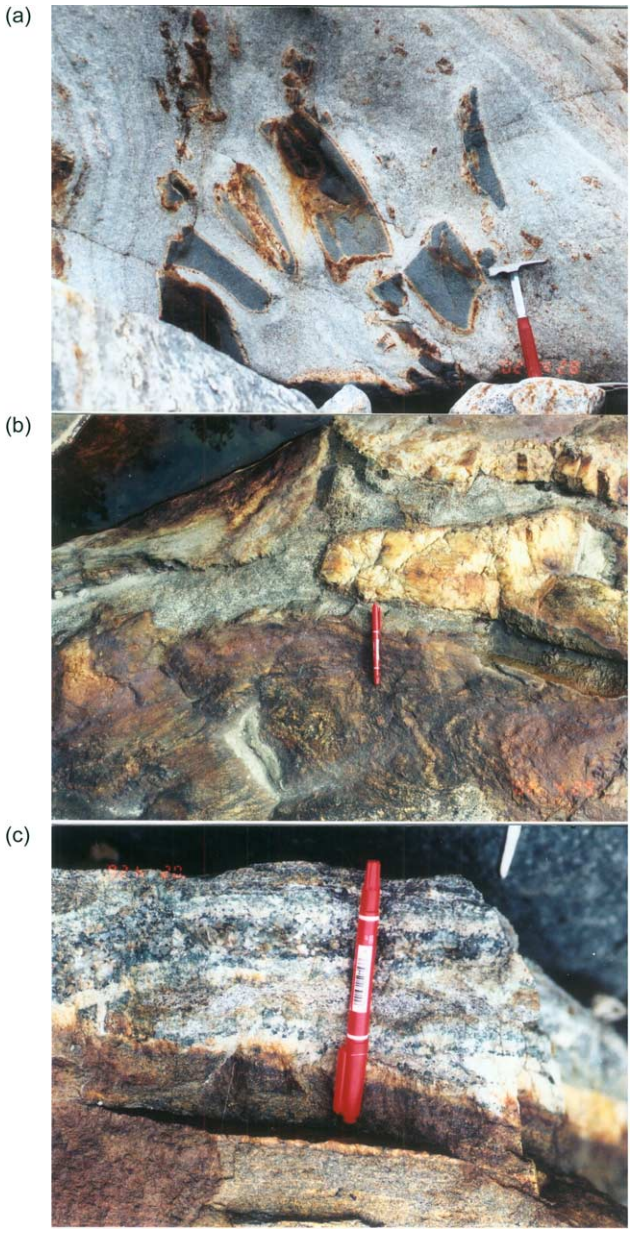

Fig. 2. Macroscopic photos of the carbonatite-like dykes. (a) Xenolith-bearing dolomitic rock from the larger dyke swarm occurring between Namche-Barwa and Giala Peri peaks. The xenoliths of the granulite facies gneisses are separated from the host rock of dolomite dyke by the light-color altered margin. (b) Carbonate-rich rocks (weathered) cutting the granulite country rocks from the larger dyke swarm. (c) Carbonate-rich dyke hosted in the granulite facies gneisses. From the centre to the rim the size of mineral grains decreases.

A second type of dyke is characterized by MgO-rich ultramafic rocks occurring as small dyke-like bodies in the granulitic terrain or as ball-shaped inclusions in diorite dykes. This third group of dyke rocks is biotite-bearing diorites.

Detailed mapping has revealed that the carbonate-rich dykes occur beneath the Greater Himalayan Crystallines and above the upper Lesser Himalayan Crystallines (Fig. 1a and b). Typically a larger carbonate-rich dyke swarm was observed at the bottom of the Greater Himalayan Crystallines.

3. Petrology and mineralogy

The mineralogical information on the rocks resulted from investigations with the polarizing microscope and, for selected samples, with the electron microprobe. For the latter a Cameca SX100 electron microprobe with five wavelength-dispersive spectrometers was used to determine the concentrations of F, Na, Mg, Al, Si, K, Ca, Ti, Cr, Mn, Fe, Ni and Ba. Counting times were 15 s at the peak and on the background (except for Na: 30 s). Natural minerals, glasses (e.g. Ba glass for the BaLα_1-peak), and pure oxides were used as standards. The applied acceleration voltage and electric current were 15 kV and 15 nA, respectively. Beam diameter was about 2 μm. The PaP correction procedure provided by Cameca was applied. The energy-dispersive system of the microprobe served as a mean of identification of phases during the selection of spots for full analyses. Selected samples for this study are listed in Table 1. Mineralogical results are shown in Table 2.

3.1. Dolomitic dykes

The central parts of the dolomitic dykes consist mainly of dolomite, with accessory magnesite and strontianite and very rare non-carbonate minerals. However, from centre to margin of the dykes, the total contents of the non-carbonate minerals increase from near zero to 20% in volume and the modal content of dolomite decreases with increasing modal content of calcite. Dolomite is close to stoichiometric composition with minor Ni and Cr contents (Table 2, sample 610). The grains define a mildly porphyroclastic texture.

Most non-carbonate minerals are olivine, spinel and phlogopite. Olivine grains usually occur as round or euhedral microphenocrysts or phenocrysts, which usually contain minute inclusions. Calcite grains commonly occur together

Table 1
Selected samples investigated for this study

Geographical location		Sample No.	Sampling location	Rock type
Collected from the larger dyke swarm between the two peaks along Yarlung Zangbo river		401	Centre of dyke	Dolomitic
	Single dyke	601	Centre of dyke	Dolomitic
		603	Centre of dyke	Sacpolite hornblendite
		610	Centre of dyke	Dolomitic
		901	Centre of dyke	Dolomitic
		902	Centre of dyke	Dolomitic
		903	Centre of dyke	Calcitic
		904	Centre of dyke	Dolomitic
		905	Centre of dyke	Calcitic
Collected from the smaller dyke swarm above the MCT1		1606	Country rock	Gneiss
	Single dyke	1612	Between dyke and gneiss	Alkali-altered rock
		1616	Margin of dyke	Dolomitic
		1617	Margin of dyke	Dolomitic
		1618	Centre of dyke	Dolomitic
		1619	Centre of dyke	Dolomitic
		1608	Centre of dyke	Dolomitic
		1630	Middle of dyke	Dolomitic
	Single dyke	1623	Between dyke and gneiss	Altered rock
		1625	Centre of dyke	Calcitic

with olivine grains. Furthermore, the amount of modal calcite shows a positive correlation with modal olivine in the dykes. All olivine in this rock is rich in the forsterite component (Fo = 94–99) with very low Ni content (Table 2), unlike that of most mantle rocks, but similar to that of most high-temperature marbles. Spinel is greenish-black in colour, rich in Mg and poor in Cr (Table 2), also unlike spinel from the mantle, but similar to that in the country rocks (Liu and Zhong, 1997). Phlogopite laths have a narrow compositional range with high X(Phl) (0.93–0.95, $X(Phl) = Mg^{2+}$/total cations in octahedral site), low Ti and Fe, and minor Ni and Cr (Table 2). Accessory non-carbonate minerals are abundant in the dolomitic bodies. Astrophyllite, apatite, zircon, garnet, pargasite, geikielite-ilmenite, C-rich warwickite, pyrite-pyrrhotite and celestine-barite were observed. Geikielite crystals usually contain Mn. From centre to margin, the Mg and Mn contents decrease, coincident with an increase of the Fe content (Table 2, sample 610). Apatite and zircon occur as inclusions of up to several tens of micrometres in size in large dolomitic grains. Celestine appears as irregular grains among or as inclusions in dolomite crystals. Eutectic textures consisting of euhedral olivine, spinel, and C-rich warwickite microphenocrysts are also observed in the rocks. The 'chilled margin' consists mainly of fine-grained calcite + spinel + olivine + phlogopite + rutile + K-feldspar + ilmenite + scapolite + wollastonite ± dolomite.

3.2. Calcitic dykes

The calcitic dykes are usually fine grained. No dolomite was found in this rock type. The non-carbonate constituents (30% mode) consist mainly of diopside, amphibole, wollastonite, anorthite, garnet, mica, and K-feldspar. Accessory minerals include apatite, zircon, scapolite, and titanite. The wollastonite and anorthite phenocrysts are usually zoned. The mineral assemblage is similar to those found in high-temperature metamorphic carbonate rocks of sedimentary origin (Le Bas et al., 2002). Additionally, the mafic minerals in this rock type commonly have minor Ni and Cr, and the mica is also phlogopite (X(Phl) = 0.85–0.90), also unlike those in the country rock represented by the granulitic gneiss of Table 2 (samples 1625 and 1606).

3.3. Scapolite hornblendite

The scapolite hornblendite is medium grained and grey to black in colour. It consists of amphibole, scapolite, as well as accessory phlogopite, magnetite, pyrite, titanite, apatite, and calcite. The square to hexagonal-sectioned scapolite grains are settled in compact aggregates of prismatic to acicular amphibole. The magnetite, pyrite, and apatite are enclosed in amphiboles or set among grains between amphibole and scapolite. Calcite occurs as interstitial grains among amphibole and scapolite. Most

Table 2
Representative mineral compositions of carbonate dykes and related rocks

Sample No.	610						603		1612				1618			1623				1625				1606			
Rock type	Dolomitic dyke						Scapolite hornblendite		Alkali-altered rock				Dolomitic dyke			Altered rock				Calcitic dyke				Country rock			
Minerals	Ol	Phl	Spn	Dol	Gei rim	Gei core	Scp[a]	Hbl	Di	Kfs	Tr	Ab	Ol	Spn	Gei	An	Di	Bt	Wo	Kfs	Di	Tr	Phl	Cpx	Pl(h)	Or(e)	Bt
SiO_2	41.90	41.64	0.01		0.01	0.00	44.83	39.37	53.6	64.95	55.59	66.62	41.36	0.02	0.05	44.69	52.86	37.67	50.94	64.80	54.09	55.87	38.37	53.44	62.59	63.90	36.76
TiO_2	0.01	1.25	0.14	0.05	57.11	61.39	0.02	1.99	0.1	0.05	0.24	0.00	0.02	0.13	61.41	0.00	0.07	3.02	0.03	0.03	0.15	0.04	0.26	0.06	0.04	0.06	4.70
Al_2O_3	0.00	13.89	63.32		0.02	0.00	28.43	16.80	1.1	18.55	1.51	21.32	0.00	68.57	0.04	35.49	1.29	15.76	0.01	18.73	0.83	1.95	16.95	0.80	23.49	19.02	13.91
Cr_2O_3	0.03	0.02	0.18		0.00	0.10	0.00	0.09	0.00	0.01	0.02	0.00	0.05	0.05	0.07	0.02	0.06	0.13	0.00	0.01	0.10	0.05	0.03	0.00	0.01	0.04	0.07
MgO	52.99	27.38	24.46	22.92	15.55	23.56	0.03	10.94	13.81	0.02	17.06	0.00	56.13	25.96	22.51	0.00	14.97	18.47	0.07	0.01	15.90	19.96	23.41	13.74	0.00	0.00	13.64
CaO	0.01	0.02	0.00	30.71	0.01	0.00	18.83	12.07	23.61	0.00	12.76	0.00	0.04	0.04	0.06	19.31	25.38	0.00	47.28	0.00	25.21	13.54	0.04	23.34	4.31	0.07	0.02
MnO	0.08	0.01	0.05	0.09	1.04	3.07	0.01	0.18	0.29	0.02	0.40	0.03	0.17	0.11	3.41	0.02	0.13	0.13	0.18	0.05	0.13	0.06	0.05	0.22	0.00	0.00	0.23
FeO	5.14	0.35	12.37	0.20	26.28	12.33	0.16	13.06	6.94	0.19	9.84	0.11	1.73	3.88	11.54	0.16	5.50	10.41	0.49	0.07	4.11	6.16	5.02	7.81	0.12	0.06	17.05
NiO	0.03	0.02	0.04	0.02	0.03	0.02	0.00	0.04	0.00	0.00	0.00	0.08	0.04	0.06	0.00	0.00	0.00	0.00	0.04	0.00	0.10	0.00	0.00	0.00	0.00	0.00	0.00
Na_2O	0.02	0.84	0.01	0.02	0.01	0.01	2.66	2.67	0.48	0.49	0.32	11.26	0.00	0.03	0.01	0.58	0.16	0.15	0.02	0.56	0.21	0.09	0.14	0.42	9.59	1.79	0.14
K_2O	0.00	9.91	0.00	0.04	0.00	0.00	0.10	1.09	0.00	16.12	0.04	0.15	0.00	0.00	0.00	0.03	0.00	9.86	0.00	15.84	0.00	0.03	10.19	0.00	0.30	14.30	9.47
Total	100.2	95.3	100.6	54.1	100.1	100.5	95.9[a]	98.29	99.9	100.4	97.8	99.6	99.5	98.9	99.1	100.3	100.4	95.6	99.1	100.1	100.8	97.7	94.5	99.8	100.5	99.3	96.0
O	4	12	4		3	3	24	23	6	8	23	8	4	4	3	8	6	12	6	8	6	23	12	6	8	8	12
Si	1.00	2.90	0.00		0.00	0.00	6.86	5.81	1.99	2.99	7.88	2.93	0.98	0.00	0.00	2.06	1.94	2.75	1.99	2.99	1.97	7.79	2.76	1.99	2.77	2.96	2.76
Ti	0.00	0.07	0.00		0.96	0.98	0.00	0.22	0.00	0.00	0.03	0.00	0.00	0.00	1.00	0.00	0.00	0.17	0.00	0.00	0.00	0.00	0.01	0.00	0.00	0.00	0.26
Al	0.00	1.14	1.84		0.00	0.00	5.14	2.92	0.05	1.01	0.25	1.10	0.00	1.97	0.00	1.93	0.06	1.36	0.00	1.02	0.04	0.32	1.43	0.04	1.22	1.04	1.23
Cr	0.00	0.00	0.00		0.00	0.00	0.00	0.01	0.00	0.00	0.00	0.00	0.00	0.00	0.00	0.00	0.00	0.01	0.00	0.00	0.00	0.01	0.00	0.00	0.00	0.00	0.00
Mg	1.89	2.84	0.90		0.52	0.74	0.00	2.41	0.76	0.00	3.61	0.00	1.99	0.94	0.73	0.00	0.82	2.01	0.00	0.00	0.86	4.15	2.50	0.76	0.00	0.00	1.53
Ca	0.00	0.00	0.00		0.00	0.00	3.12	1.91	0.94	0.00	1.94	0.00	0.00	0.00	0.00	0.95	1.00	0.00	1.98	0.00	0.98	2.02	0.00	0.93	0.20	0.00	0.00
Mn	0.00	0.00	0.00		0.02	0.06	0.00	0.02	0.01	0.00	0.05	0.00	0.00	0.00	0.06	0.00	0.00	0.01	0.01	0.00	0.00	0.01	0.00	0.01	0.00	0.00	0.01
Fe^{3+}			0.15		0.07	0.04		0.23	0.00		0.00			0.03	0.00		0.07		0.02		0.04	0.00		0.01			
Fe	0.10	0.02	0.11		0.42	0.18	0.02	1.38	0.21	0.01	1.17	0.00	0.03	0.05	0.21	0.01	0.10	0.64	0.00	0.00	0.09	0.72	0.30	0.23	0.00	0.00	1.07
Ni	0.00	0.00	0.00		0.00	0.00	0.00	0.00	0.00	0.00	0.00	0.00	0.00	0.00	0.00	0.00	0.00	0.00	0.00	0.00	0.00	0.00	0.00	0.00	0.00	0.00	0.00
Na	0.00	0.11	0.00		0.00	0.00	0.79	0.76	0.04	0.04	0.09	0.96	0.00	0.00	0.00	0.05	0.01	0.02	0.00	0.05	0.02	0.02	0.02	0.03	0.82	0.16	0.02
K		0.88					0.02	0.21		0.95	0.01	0.01				0.00		0.92		0.93		0.01	0.94		0.02	0.85	0.91

Symbols for mineral abbreviations are after Kretz (1983) except Gei, Pl(h) and Or(e), symbols for geikielite, Pl and Or in antiperthite, respectively. Fe^{3+} in Ol, Di, Wo, Ilm, Gei and Spn, and in Hbl and Tr are calculated after Droop (1987) and Leake et al. (1997), respectively. Fe in Bt, Pl, Opx, Phl, An and Scp is regarded as Fe^{2+}.

[a] Total includes 0.82 wt% SO_2.

amphibole is pargasite with minor Cr and Ni contents. It shows no significant compositional variation (Table 2). The scapolite formula was calculated by normalizing to Si + Al = 12 apfu (atoms per formula unit), as recommended by Teertstra and Sherriff (1997). All scapolite compositions indicate meionite (classification after Teertstra and Sherriff, 1997) with minor Cr, Mg and Mn contents. The contents of Fe and S are generally low (0.02 and 0.12 apfu, respectively), and the Si values are below 7.3 apfu (Table 2). Thus, the scapolite is similar to that found in skarns.

3.4. Altered halos

Three types of alteration halos mantling the carbonate dykes were distinguished. The most common is an alkali-altered rock, consisting of diopside + tremolite + K-feldspar + albite + calcite with reddish-brown allanite, apatite, epidote, and titanite as accessory minerals. It occurs close to the dolomite rock, scapolite hornblendite and scapolite glimmerite, ranging from fine to coarse grained with granoblastic texture and varying from 10 cm to 1 m in width. The diopside grains coexist with potassium feldspar and albite. The reddish-brown REE-rich allanite occurs as fine-grained aggregate within or around albite grains. Calcite commonly forms the matrix. K-feldspar is strongly potassic (95% orthoclase) compared to that of the granulites (Table 2). Albite is almost pure (99% albite). The mineral assemblage is similar to that of fenites (e.g. Le Bas, 1981; Woolley, 1982; Lentz, 1998).

The second type of alteration is a rock composed of wollastonite + calcite + anorthite + diopside + scapolite ± K-feldspar. Biotite, titanite and apatite are common accessory minerals. This rock occurs close to the calcite dykes. It is fine to medium grained possessing granoblastic textures and varies from 10 to 80 cm in width. Calcite also occurs as cementing groundmass. K-feldspar is similar to that of the first altered rock type. In addition, the mafic constituents of both rocks types, such as diopside, wollastonite, tremolite, and biotite, usually have minor contents of Cr or Ni, different from those in the granulite facies country rocks (Table 2).

The third type of alteration is a rock consisting of epidote, chlorite, quartz, calcite, and amphibole. It occurs at the outermost part of the alteration zones around the carbonate dykes and is 10–50 cm wide.

4. Geochemistry

All samples investigated for bulk rock composition were broken into small fragments up to 3 cm in size and further crushed into smaller fragments about 1 cm in size using a jaw-crusher. The smaller fragments were cleaned with deionized water, dried in an oven at 50 °C, and then ground to powder (200 mesh) using a tungsten carbide pulverizing swing mill.

The major-element compositions were determined using wet chemical analysis at University of Geosciences (Beijing). For the determination of the concentrations of about 30 trace elements (REE and others), rock powder (50 mg) was dissolved in ultrapure $HF + HNO_3$. The dissolution process was performed in closed teflon containers in a microwave oven at temperatures up to 230 °C. The finally obtained solution (rock:solution = 1:1000) was used to determine the concentration of trace elements with a high resolution ICP-MS (VG AXIOM) at Universität Karlsruhe. Calibration lines were defined for each isotope using standard solutions with known element concentrations. In addition to, the samples, procedural blanks and certified geostandards were determined in three independent runs. Variations in signal intensity were corrected by means of internal standards. For each rock sample the entire process described above was performed twice. Precision was generally better than 3% for each element and the results on the reference samples were within ±10% of the certified values. In addition, ICP-MS analyses were undertaken with a Finnigan ELEMENT instrument at the Institute of Geology and Geophysics, CAS. The quality of these analytical data was checked against Chinese standards (GSR1-GSR6) and several Japanese standards. Selected analyses of samples at the different laboratories are given in Tables 3a and b. These results acquired at different laboratories are consistent and, thus, suggest that they are accurate.

Sr and Nd isotopic ratios were determined using a Finnigan MAT262 multi-collector spectrometer operated in static mode. $^{87}Sr/^{86}Sr$ and $^{143}Nd/^{144}Nd$ ratios were measured on single Ta filaments and on double Ta–Re filament assemblages, respectively. After digestion in HF–HNO_3, Sr and total REE were eluted with 2.5 and 6 M HCl from cation exchange columns packed with 6 ml of AG 50W, 200–400# resin. Nd was purified on Teflon-supported HDEHP eluted with 0.4 M HCl. $^{87}Sr/^{86}Sr$ ratios were normalized to $^{86}Sr/^{88}Sr = 0.1194$. An average $^{87}Sr/^{86}Sr$ value of 0.710239 ± 0.000009 was obtained for the NBS-987 standard. $^{143}Nd/^{144}Nd$ ratios were normalized to $^{146}Nd/^{144}Nd = 0.7219$. An average $^{143}Nd/^{144}Nd$ value of 0.511860 ± 0.000013 was obtained for the La Jolla standard.

For carbon and oxygen isotope determination, powdered bulk samples were treated with 100% phosphoric acid. The liberated CO_2 was captured off-line in sample tubes after cryogenic cleaning. Measurements were achieved using a Finnigan MAT 252 mass spectrometer. Analytical details can be found in Al-Aasm et al. (1990). The measured isotope ratios were calibrated using a Chinese carbonate standard, GBW04405, with a $\delta^{18}O_{PDB}$ and $\delta^{13}C_{PDB}$ value of 0.58‰ and −8.49‰, respectively. All $\delta^{18}O$ and $\delta^{13}C$ values are given in ‰ deviation relative to V-SMOW and V-PDB, respectively. The reproducibility of both δ values is typically to be better than ±0.2‰. Selected Sr, Nd, C and O isotopic data are listed in Table 4.

Table 3a
Representative whole-rock compositions of carbonate dykes and related rocks and typical magnesiocarbonatite compositions for comparison

Sample	401	601	603	610	901	902	903	904	905	1612	1616	1618	1630	1623	1625	1606	ZD-13	ZS-1	ZS-2	ZS-4
SiO_2 (wt%)	0.89	1.15	36.9	4.65	0.06	1.81	7.26	10.38	13.88	52.58	9.58	10.35	11.23	45.90	12.74	70.89	0.51	0.00	0.00	0.00
TiO_2	0.02	0.06	1.92	0.05	0.01	0.02	0.09	0.10	0.21	0.44	0.08	0.06	0.08	1.01	0.12	13.60	0.00	0.04	0.01	0.10
Al_2O_3	0.62	0.95	16.6	0.65	0.11	0.34	1.59	2.83	0.83	9.04	1.18	1.17	1.37	17.04	2.50	0.94	0.00	0.00	0.00	0.00
Fe_2O_3	0.02	0.04	5.32	0.09	0.02	0.04	0.08	0.04	0.07	0.93	0.01	0.01	0.14	0.84	0.15	5.57	2.76	4.30	3.92	6.82
FeO	0.28	0.48	6.84	0.26	0.25	0.37	1.12	1.33	1.29	4.14	0.97	0.91	1.11	2.98	0.86	2.78				
MgO	22.59	21.71	10.0	21.4	22.9	22.6	2.47	21.0	2.92	9.66	18.17	22.63	23.11	7.84	3.18	0.75	14.87	18.78	17.65	16.87
CaO	29.55	29.64	12.9	30.0	29.3	29.2	49.0	32.7	46.5	15.43	35.49	31.53	30.43	20.90	46.68	1.72	35.31	31.43	33.46	31.61
Na_2O	0.09	0.14	2.78	0.12	0.09	0.11	0.25	0.11	0.21	2.41	0.07	0.11	0.07	0.43	0.20	2.63	0.07	0.04	0.05	0.01
K_2O	0.03	0.05	1.12	0.38	0.03	0.03	0.55	0.03	2.82	1.50	0.17	0.13	0.04	0.48	0.40	0.96	0.00	0.00	0.00	0.00
P_2O_5	0.00	0.00	0.15	0.00	0.00	0.00	0.00	0.00	0.04	0.34	0.08	0.07	0.05	0.17	0.16	0.07	0.55	4.00	5.39	0.03
MnO	0.02	0.04	0.09	0.01	0.01	0.01	0.01	0.04	0.07	0.13	0.02	0.07	0.03	0.06	0.03	0.09	0.54	0.20	0.16	0.24
LOI	45.76	45.49	4.57	41.8	46.7	44.8	37.3	31.6	31.5	2.86	33.42	32.15	31.99	2.47	32.70	0.38	43.81	40.43	38.55	43.30
Total	99.9	99.8	99.2	99.4	99.4	99.3	99.7	100.2	100.3	99.5	99.2	99.2	99.7	100.1	99.7	99.9	98.76	99.38	99.33	99.12
Sc (ppm)	0.28	0.49	61.6	0.52	0.06	0.21	2.03	2.38	3.40	7.68	1.10	0.58	1.11	18.8	2.76					
V	10.9	13.1	408	11.2	8.23	11.1	11.4	10.6	20.7	18.9	9.23	21.4	11.8	63.8	0.00	159	22	34	28.0	34.0
Cr	0.04	2.70	333	1.00	0.00	0.00	1.91	0.00	14.7	27.8	0.00	2.69	0.00	82.4	9.69	69.1	0	6.0	5.0	3.0
Co	2.99	6.45	78.2	3.58	1.50	2.76	3.95	8.53	9.90	24.6	5.57	7.01	6.79	28.0	4.95	20.7				
Ni	7.8	8.14	172	7.37	6.73	6.69	10.9	11.1	17.7	45.2	9.06	9.07	9.04	52.8	49.1	41.8	0	0	0	7.0
Cu	0.7	0.65	368	0.25	0.00	1.10	3.68	4.62	6.40	12.8	1.94	0.05	66.3	36.3	1.86					
Zn	8.87	11.39	111	9.74	4.60	6.60	4.43	0.00	11.9	49.8	0.00	55.5	5.83	52.5	13.6					
Rb	0.6	1.5	28.1	9.45	0.37	1.87	23.8	0.00	20.1	74.4	6.01	5.06	1.16	26.6	12.9		0	0	0	0
Sr	55.3	54.4	122.0	94.4	59.6	57.3	279	2629	221	119	65.4	67.9	99.6	274	391	60.8	2515	2061	1823	1966
Y	3.1	3.7	35.1	3.48	2.37	3.38	11.2	8.25	14.4	58.7	8.32	3.09	4.70	41.4	7.3	34.0	19	15	23	0
Zr	2.2	6.5	56.0	12.2	0.5	2.4	13.0	41.4	24.6	10.7	35.7	12.9	35.2	34.7	6.5	276	108	102	248	99
Nb	0.48	0.60	5.68	0.86	0.02	0.25	2.53	2.64	4.69	10.5	2.27	0.95	2.18	20.1	1.47	12.4	6	7	6	14
Ba	5.20	2.97	46.2	236	2.16	5.53	47.4	19.7	223	246	313	14.7	34.7	80.8	241		368	121	138	415
La	1.98	2.60	7.40	4.46	1.70	2.07	11.0	11.3	18.5	99.8	10.3	2.98	5.19	24.3	7.11	56.2	41	18	15	2
Ce	3.22	4.01	18.1	7.32	2.81	3.43	20.2	24.4	31.1	174	19.2	5.60	10.2	62.7	13.9	115	58.8	45.2	36.6	6.5
Pr	0.47	0.55	2.79	0.86	0.39	0.50	2.31	2.61	3.73	17.6	2.15	0.66	0.93	8.24	1.63	13.4	5.9	7.2	5.0	0.9
Nd	1.88	2.20	14.3	3.22	1.50	2.02	8.40	9.62	13.3	71.3	7.44	2.62	2.86	32.6	6.43	51.2	19.5	30.9	23.9	4.2
Sm	0.39	0.47	4.46	0.71	0.29	0.44	1.81	1.78	2.65	10.6	1.73	0.55	0.79	7.51	1.31	10.1	3.2	7.3	6.0	0.8
Eu	0.09	0.10	1.59	0.19	0.07	0.10	0.36	0.33	0.60	1.79	0.40	0.10	0.20	1.53	0.32	1.58	1.1	2.4	2.3	0.3
Gd	0.44	0.53	6.18	0.63	0.33	0.50	1.87	1.68	2.69	10.1	1.56	0.53	0.80	7.61	1.19	8.99	3.2	6.6	7.1	0.9
Tb	0.06	0.08	1.04	0.09	0.05	0.08	0.31	0.27	0.40	1.66	0.23	0.08	0.13	1.29	0.20	1.28				
Dy	0.41	0.48	6.73	0.54	0.27	0.44	1.79	1.52	2.23	9.84	1.28	0.47	0.75	7.40	1.18	6.31	3.1	4.1	5.7	0.5
Ho	0.08	0.10	1.41	0.12	0.06	0.09	0.35	0.28	0.43	1.94	0.25	0.10	0.15	1.40	0.24	1.27	0.6	0.6	0.9	0.1
Er	0.23	0.27	4.02	0.31	0.17	0.26	0.97	0.81	1.18	5.87	0.68	0.29	0.41	4.00	0.71	3.50	1.5	1.2	1.7	0.2
Tm	0.03	0.04	0.57	0.04	0.02	0.03	0.16	0.14	0.19	0.88	0.12	0.04	0.08	0.58	0.13	0.55				
Yb	0.17	0.25	3.70	0.29	0.13	0.20	0.94	0.86	1.13	5.18	0.71	0.24	0.47	3.36	0.74	3.60	1.4	0.7	1.0	0.2
Lu	0.02	0.03	0.53	0.04	0.02	0.03	0.14	0.12	0.16	0.75	0.11	0.04	0.07	0.48	0.11	0.60	0.2	0.1	0.1	0.0
total REE	9.5	11.7	72.8	18.8	7.81	10.2	50.6	55.8	78.3	411	46.2	14.3	23.1	163	35.2	274	139.5	124.3	105	16.6
Hf	0.08	0.21	2.49	0.41	0.01	0.08	0.21	1.10	0.69	0.76	0.80	0.43	1.01	1.69	0.20	7.33				
Th	0.45	1.49	4.12	1.10	0.02	0.38	4.06	4.12	5.70	13.9	2.49	0.88	1.18	14.1	2.48	29.2	0	0	1	4
U	0.18	0.21	2.16	0.23	0.02	0.24	0.56	2.01	0.65	6.57	0.27	0.86	0.34	7.56	3.47	2.85	1	2	0	3

ZS-1, 2, 4 and 13 are after Harmer et al. (1998).

Table 3b
Trace element concentrations in carbonate dykes and related rocks from the eastern Himalayan syntaxis

Sample	401	601	603	610	901	902	903A	903B	904	905	1608	1612	1616	1618	1625	1630
Sc	0.37	3.29	53.7	3.17	1.76	1.70	3.57	5.71	4.06	8.17	1.84	11.0	3.64	3.04	4.74	3.85
V	b.d.l.	2.89	376	6.52	0.51	3.26	12.4	13.4	10.9	26.1	5.72	52.3	10.0	12.7	17.2	15.9
Cr	0.55	3.55	349	5.91	1.54	1.64	13.8	11.7	9.71	30.0	2.71	32.9	6.90	3.69	14.3	5.64
Mn	1.01	317	763	109	178	204	162	153	319	715	397	1056	220	580	316	421
Co	0.11	6.09	86.9	3.54	1.11	2.42	3.90	3.56	8.55	10.8	2.66	26.2	5.26	6.45	4.98	8.22
Ni	0.99	2.02	140	2.74	1.21	1.40	7.23	4.49	6.40	13.4	1.71	11.8	5.03	2.21	8.79	5.35
Cu	2.83	1.83	312	0.92	1.05	1.51	11.13	5.71	4.60	8.87	2.33	52.3	4.45	1.88	5.85	6.02
Zn	6.37	7.38	66.8	10.2	4.90	8.94	29.6	11.1	10.1	28.4	15.6	64.3	25.9	38.1	29.6	36.2
Ga	b.d.l.	0.40	26.6	1.54	b.d.l.	0.18	3.31	3.35	2.57	14.1	0.48	22.7	3.08	0.91	11.8	2.03
Rb	0.03	1.47	32.6	12.3	0.38	2.01	27.2	29.4	0.28	31.4	7.42	67.2	9.06	5.51	17.2	2.49
Sr	0.85	53.3	117	88.3	55.0	49.4	251	284	2423	230	56.8	127	59.5	61.7	420	98.2
Y	b.d.l.	3.76	31.3	4.41	2.69	3.78	12.2	13.8	9.49	18.1	1.56	57.2	10.3	3.58	10.3	7.03
Zr	1.18	23.4	66.8	29.1	18.4	2.23	82.8	5.17	46.1	29.1	3.62	76.0	69.6	12.8	98.6	113
Nb	0.43	1.02	6.64	1.66	0.54	0.69	3.61	2.66	2.29	12.7	0.76	14.0	2.24	1.37	3.27	2.83
Cs	b.d.l.	b.d.l.	22.0	b.d.l.	b.d.l.	b.d.l.	0.24	0.27	b.d.l.	b.d.l.	0.14	2.19	b.d.l.	0.26	b.d.l.	b.d.l.
Ba	1.86	6.49	46.5	33.5	4.73	7.48	63.9	46.1	9.14	246	17.1	231	69.8	15.6	238	33.1
La	2.51	3.10	6.57	5.64	2.17	3.04	19.9	15.9	14.9	22.3	2.14	106	15.6	7.35	10.3	6.72
Ce	4.34	5.04	18.1	8.62	3.82	4.57	23.5	24.3	29.9	39.1	4.18	191	30.0	7.41	19.0	15.4
Pr	0.61	0.65	2.62	1.08	0.50	0.64	3.00	3.02	3.34	4.65	0.48	19.2	3.52	0.91	2.19	1.82
Nd	2.67	2.74	13.8	4.13	1.92	2.57	11.1	11.2	12.2	17.5	1.81	68.3	12.7	3.26	7.68	6.24
Sm	0.55	0.58	4.38	0.79	0.40	0.59	2.34	2.36	2.39	3.53	0.38	13.6	2.57	0.74	1.76	1.39
Eu	0.12	0.13	1.58	0.15	0.09	0.13	0.42	0.42	0.39	0.68	0.11	2.19	0.43	0.13	0.33	0.26
Gd	0.53	0.56	5.32	0.68	0.38	0.57	1.97	2.03	1.89	2.88	0.30	10.7	2.07	0.60	1.45	1.11
Tb	0.10	0.09	0.94	0.11	0.07	0.09	0.36	0.35	0.34	0.47	0.05	2.00	0.35	0.11	0.27	0.21
Dy	0.48	0.51	5.89	0.63	0.36	0.55	2.03	1.98	1.80	2.59	0.29	11.4	1.87	0.66	1.58	1.21
Ho	0.11	0.11	1.24	0.14	0.08	0.12	0.42	0.41	0.36	0.52	0.06	2.37	0.38	0.14	0.34	0.26
Er	0.30	0.30	3.55	0.38	0.22	0.33	1.24	1.19	1.07	1.51	0.19	7.30	1.11	0.41	1.03	0.80
Tm	0.05	0.04	0.48	0.05	0.03	0.04	0.17	0.16	0.15	0.20	0.03	1.03	0.15	0.05	0.15	0.12
Yb	0.23	0.25	3.11	0.34	0.17	0.27	1.07	0.99	0.94	1.24	0.16	6.86	0.96	0.37	0.98	0.80
Lu	0.04	0.04	0.45	0.05	0.03	0.04	0.16	0.14	0.14	0.17	0.02	0.95	0.14	0.05	0.15	0.12
Hf	0.07	0.81	3.27	1.08	0.68	0.13	2.80	0.35	1.81	1.25	0.18	3.00	2.05	0.60	2.60	3.37
Ta	0.10	0.11	0.47	0.20	0.08	0.11	0.38	0.26	0.30	0.47	0.10	2.10	0.25	0.18	0.33	0.33
Pb	22.3	3.86	20.5	6.23	3.13	2.84	11.5	8.09	10.7	13.9	5.02	30.0	4.03	3.41	10.15	5.44
Th	b.d.l.	0.21	4.59	4.70	b.d.l.	0.32	5.82	5.78	5.65	9.91	0.38	19.4	5.50	1.89	4.77	2.13
U	0.02	0.12	2.46	0.79	0.11	0.42	1.45	0.99	3.40	1.12	0.16	7.36	0.78	2.15	4.64	0.68

b.d.l., below detection limit.

4.1. Dolomitic dykes

The dolomite-rich dykes show relative high MgO, low SiO_2, Al_2O_3, CaO and alkali contents compared to the average magnesiocarbonatite composition given by Woolley and Kempe (1989). In comparison with other mantle-derived dolomitic carbonatites, e.g. those of southeast Zambia (Bailey, 1989) and Buhera district, SE Zimbabwe (Harmer et al., 1998), the dolomitic dykes here are also enriched in MgO and depleted in CaO (Tables 3a and b). Specifically, the MgO and CaO contents of the dolomite rocks are similar to those of stoichiometric dolomite (Tables 3a and b). The concentrations of most incompatible elements, e.g. REEs, in the rocks are remarkably low (Tables 3a and b). The total REE contents of the rocks are typically below 60 ppm. From centre to margin of the dykes, the MgO content decreases with increasing contents of SiO_2, Al_2O_3 and CaO (Table 3a, e.g. samples 1618 and 1616), consistent with the modal proportions of the non-carbonate minerals. The coarse-grained central portions of the dykes generally have lower concentrations of incompatible elements than the fine-grained marginal parts. However, the REE patterns, in the chondrite-normalized plots of Fig. 3a and b, are perfectly parallel to each other. Moreover, all dolomitic dykes here have similar REE chondrite-normalized patterns. The $^{87}Sr/^{86}Sr$, $^{143}Nd/^{144}Nd$, $\delta^{18}O$ and $\delta^{13}C$ of the dolomitic rocks range from 0.7091 to 0.7239, 0.511759 to 0.512069, 16.6 to 24.4‰, and 0.8 to 3.5 ‰, respectively (Table 4, Figs. 5 and 6). The C and O isotope values increase from centre to margin of the dykes. Moreover, the $\delta^{18}O$ values suggest an isotopic exchange with silicate country rocks, or admixing of mantle-derived fluids (Table 4, Fig. 6). $^{87}Sr/^{86}Sr$ and $^{143}Nd/^{144}Nd$ values of the central portions vary between 0.709–0.713 and 0.5117–0.5120, respectively (Table 4, Fig. 5).

4.2. Calcitic dykes

The calcite-rich dykes have relatively high SiO_2 content in the range of 7–13 wt%. The MgO and CaO contents of these dykes are also similar to those of calcite (Table 3a, samples 903, 905 and 1625). The REE concentrations of the

Table 4
Sr, Nd, C and O isotope data of carbonate dykes and related rocks

Sample No.	$^{87}Sr/^{86}Sr$	$^{143}Nd/^{144}Nd$	$\delta^{13}C_{PDB}$	$\delta^{18}O_{SMOW}$
401	0.709816±15	0.511964±17	1.30	23.1
601	0.710654±13	0.511922±15	1.40	21.9
603	0.706652±17	0.512904±16		
610	0.710676±15	0.511849±16	0.93	21.7
1612	0.732411±14	0.511927±15		
1616	0.723913±15	0.511908±15		
1617	0.723254±12	0.511937±16	3.55	20.1
1618	0.713581±17	0.512031±15	2.55	17.9
1619	0.713974±17	0.512069±16	2.86	16.6
1608	0.713750±16	0.511726±15		
1630	0.713808±14	0.512040±14	3.02	20.0
1623	0.716644±13	0.511957±16		
1625	0.710806±14	0.511907±16		
901	0.710185±16	0.511960±16		
902	0.710115±17	0.511964±15	1.68	24.4
904	0.709101±14	0.511759±15	0.80	19.3
903	0.711998±17	0.511743±16	0.90	8.0
905	0.713824±17	0.511884±16	1.10	8.0
ZD-13[a]	0.704851±15	0.512019±14		
ZS-1[a]	0.704729±16	0.512636±8		
ZS-2[a]	0.704672±14	0.512619±9		
ZS-4[a]	0.704902±17	0.512540±21		

Errors are two standard deviations (2σ) and refer to the last two digits.
[a] After Harmer et al. (1998).

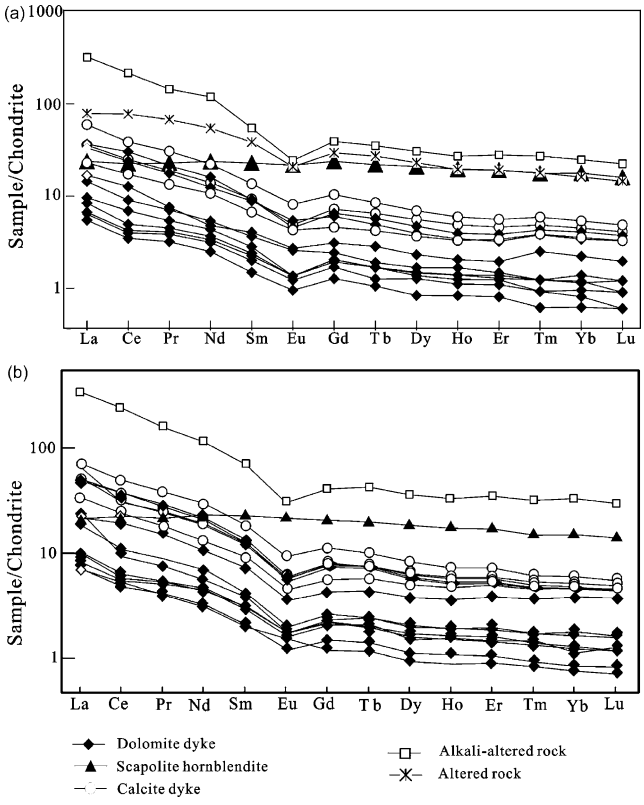

Fig. 3. Chondrite-normalized REE patterns according to Boynton (1984) for carbonatic dykes and related rocks as determined at Beijing (a), and at Universität Karlsruhe (b), respectively.

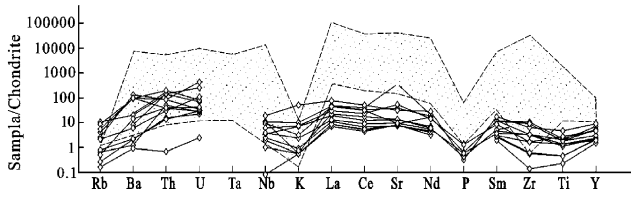

Fig. 4. Chondrite-normalized spider diagram for the carbonatite-like dykes from the eastern Himalayan syntaxis. Shaded area represents the range for carbonatites according to Nelson et al. (1988). Normalization to chondrite was achieved according to Sun and McDonough (1989).

calcite-rich dykes are somewhat higher than those of the dolomite-rich dykes (Fig. 3a and b). Nevertheless, they are clearly lower compared to typical calcite carbonatite (Woolley and Kempe, 1989). In addition, the chondrite-normalized patterns of the calcitic dykes are parallel to those of the dolomitic dykes (Fig. 3a and b), thus, differing significantly from any carbonatites (see also Fig. 4). The $^{87}Sr/^{86}Sr$ and $^{143}Nd/^{144}Nd$ ratios (Table 4, Fig. 5) of central portions of the calcitic dykes and the C isotope signatures of these dykes are similar to those of the dolomitic rocks, but their O isotope values are much lower (Table 4, Fig. 6), being close to values typical for mantle-derived carbonatites (e.g. Deines, 1989; Le Bas et al., 1992; Keller and Hoefs, 1995).

4.3. Scapolite hornblendite

Scapolite hornblendite is enriched in Al_2O_3, MgO, CaO and FeO (total) and depleted in SiO_2 compared to normal mafic rocks. Cr, Ni and Cu concentrations of the rock are relatively high (Tables 3a and b). The REE normalized pattern of the rock is flat with slightly negative Eu anomaly, thus, being different from those of the host rocks (Fig. 3a and b). Furthermore, the $^{87}Sr/^{86}Sr$ and $^{143}Nd/^{144}Nd$ ratios are similar to those of mantle rocks and again unlike those of the host rocks (Table 4, Fig. 5). These data clearly show that

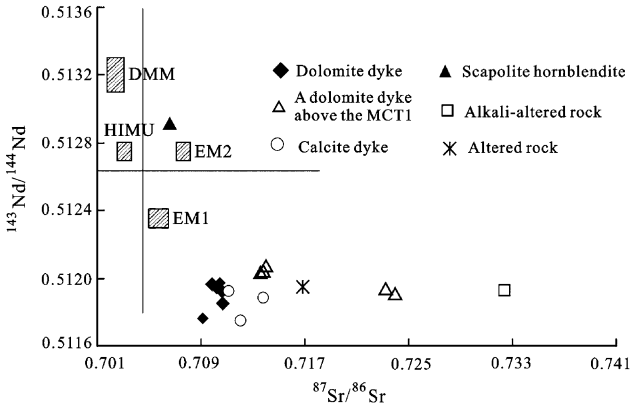

Fig. 5. Plot of $^{87}Sr/^{86}Sr$–$^{143}Nd/^{144}Nd$ data for carbonatite-like dykes and related rocks from the eastern Himalayan syntaxis (see Table 4 for data).

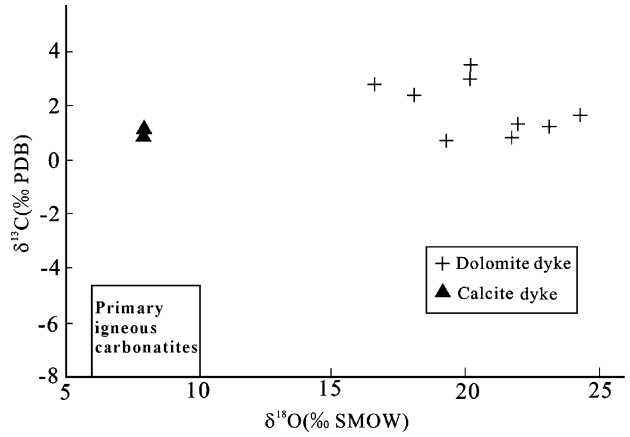

Fig. 6. Plot of $\delta^{18}O$ (SMOW)–$\delta^{13}C$ (PDB) data for carbonatite-like dykes from the eastern Himalayan syntaxis (see Table 4 for data). Box for 'primary igneous carbonatites' after Keller and Hoefs (1995).

the scapolite hornblendite has a different source relative to its host rock, even though they spatially coexist.

4.4. Altered halos

The alkali-altered rocks show much higher REE concentrations compared to the dolomitic dykes, but their chondrite-normalized patterns are similar to the dolomitic dykes. Their REE patterns are perfectly parallel to each other (Fig. 3a and b, samples 1612, 1616, and 1618) suggesting that the corresponding rocks have the same source. Compared with the country rocks, the altered rocks show relatively high MgO and CaO as well as low SiO_2 and Al_2O_3 contents (Tables 3a and b, sample 1612 and country rock). In comparison with typical fenites worldwide, the altered rocks have low abundances of alkalies as well as modal albite and K-feldspar but no aegirine or aegirine augite. The second type of the wollastonite-bearing altered rock is specially enriched in CaO, MgO and volatiles. It is depleted in SiO_2 relative to the country rock (Tables 3a and b, sample 1623 and country rock). This altered rock is similar in compositions to those found in skarn systems. The REE pattern is again parallel to those of dolomite and calcite dykes, although it has higher REE concentrations than the calcite dykes, suggesting that they are derived from similar sources (Fig. 3a and b).

The $^{87}Sr/^{86}Sr$ values of these altered rocks are markedly higher than those of the carbonate dykes. From centre to margin of these dykes and further into the altered rocks, the $^{87}Sr/^{86}Sr$ values increase markedly, whereas the $^{143}Nd/^{144}Nd$ ratios have minimal variation (Table 4, Fig. 5).

5. Geochronology

Amphibole grains from a scapolite hornblendite (sample 603) were separated using conventional techniques including hand-picking under a binocular microscope to be at least 99% pure and irradiated for 43 h at the Beijing Nuclear Research Institute Reactor. Also irradiated was a Chinese standard, ZBH25, for calculating the *J* factor, and K_2SO_4 and CaF_2 for determining the correction factors for interfering neutron reactions. All samples were step-heated using a radio-frequency furnace. Argon isotope analyses were carried out on a MM 1200 mass spectrometer at the Institute of Geology, Chinese Academy of Geological Sciences, Beijing. The results are listed in Table 5 and shown graphically as Ar/Ar age spectra and isochron plots in Fig. 7. They clearly show that the scapolite hornblendite was formed during the late Neogene. Due to the inclusion of scapolite hornblendite in the dolomitic dykes, it is assumed to be younger.

A dolomitic dyke from the larger dyke swarm and a similar rock from the smaller dyke swarm were dated using the K–Ar method. Single-crystal fragments of phlogopite were hand-picked under a binocular microscope. A Chinese standard, ZBH-25, was used for calibrating the RGA-1 mass spectrometer. The results are listed in Table 6. The K–Ar result for the larger swarm is consistent with the age

Table 5
Summary of $^{40}Ar/^{39}Ar$ results of amphibole in sample 603

Temperature °C	$^{40}Ar/^{39}Ar$	$^{36}Ar/^{39}Ar$	$^{37}Ar/^{39}Ar$	^{39}Ar (E^{-14} moles)	Age (Ma)	Error (Ma)	^{39}Ar cum %
500	44.5516	0.14870	4.56380	37.53	20.10	4.70	0.64
600	44.2825	0.14870	5.03650	17.10	15.20	4.80	0.93
700	85.2447	0.28930	7.83570	13.69	6.90	0.50	1.16
800	1.83090	0.00650	2.52130	67.40	1.63	0.21	2.29
900	5.08660	0.01760	2.51220	42.70	1.50	0.15	3.02
1000	0.93190	0.00400	4.83110	138.50	1.61	0.15	5.36
1100	21.9749	0.07470	2.64100	69.17	1.52	0.05	6.53
1200	0.95460	0.00400	4.45670	4156.10	1.53	0.07	76.64
1260	4.33030	0.01540	4.40320	477.10	1.57	0.06	84.68
1320	3.83780	0.01150	4.16440	817.40	15.44	0.18	98.46
1400	3.90880	0.01150	4.16440	90.82	16.94	0.41	100.00

J, 0.011913; weight, 0.2386 g; total age, 3.86 Ma.

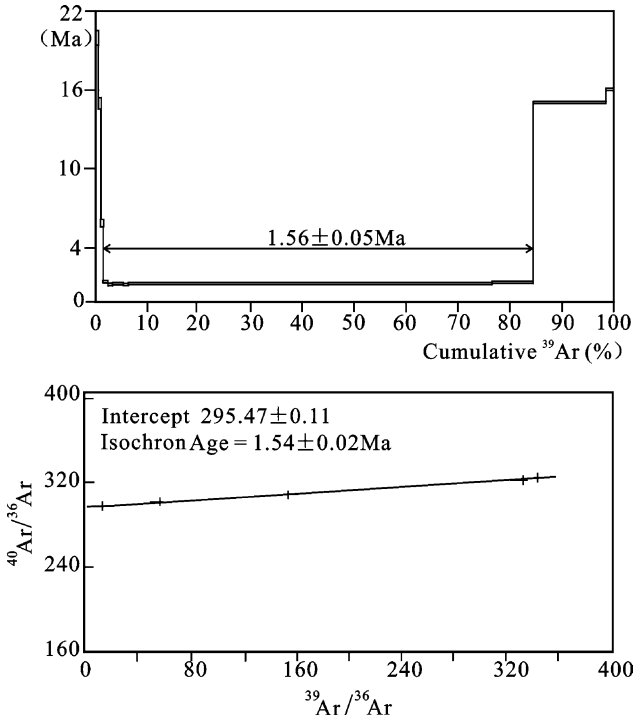

Fig. 7. ^{40}Ar/^{39}Ar release spectra and isochron diagrams of hornblende from sample 603 (see Table 5 for data).

obtained from the hornblendite, suggesting that the carbonate dykes have been formed during the late Neogene.

6. Discussion

6.1. Igneous versus sedimentary and hydrothermal origin

Compared with sedimentary carbonates and mantle-derived carbonatites worldwide (Table 7, Fig. 4), the eastern Himalayan carbonate dykes have geochemical signatures similar to some sedimentary carbonates, e.g., low contents of Sr, Ba, U, Th and REEs. However, it is likely that the carbonate-rich dykes are formed neither directly from sedimentary rocks nor as precipitates from hydrous fluids for the following reasons. Assuming that the eastern Himalayan carbonate-rich rocks represent former sedimentary layers, the entire dyke-like bodies should have experienced granulite facies metamorphism as the enclosing granulite facies gneisses. Under the derived high temperatures of $>800\,^{\circ}C$ (Liu and Zhong, 1997), sedimentary dolomites should have reacted with the surrounding pelitic rocks to produce diopside, garnet, olivine, humite, periclase and other minerals as well as a fluid phase. This would have resulted in a gradual disappearance of the dolomites. Thus, former sedimentary layers can be excluded here as it could hardly be explained by such hypothesized layers that the dykes crosscut the structure of the granulite complex. However, this would be the case when hydrothermal fluids have precipitated calcite or dolomite as well as accessory phases in dykes. However, the extended alteration zones around the dykes would be unusual for ordinary dykes formed by hydrothermal activity. In fact, the minerals of the alteration zone between the carbonate-rich dykes and granulite facies rocks, for instance, almost pure albite, are unlikely to occur in a granulite facies gneiss that contain, typically, Ca-richer plagioclases. But the altered rocks must have formed at elevated temperatures. In addition, they are similar to those around carbonatites and alkali ultramafic rocks (e.g. Tuttle and Gittins, 1966; Le Bas, 1981). Thus, the alternative explanation is that the altered rocks were formed by carbonate melts reacting with the granulite facies gneisses after they had been already significantly cooled.

The most important arguments for an igneous formation of the dykes come from field and microscopical observations. Field mapping has revealed that the eastern Himalayan carbonate dykes have typical characteristics of igneous rocks. They carry xenoliths and show chilled margins and alteration halos (Fig. 2). Microscopical textures, such as zoned minerals and mineral intergrowth in interstices (eutectic crystallization) reported above, also point to crystallization from a melt. In contrast to sedimentary carbonate-rich rocks, typically showing high ^{87}Sr/^{86}Sr ratios (e.g. Harris et al., 2003; Evans et al., 2001; Blum et al., 1998; Krishnaswami et al., 1992), the eastern Himalayan carbonate-rich rocks show little radiogenic Sr. But more importantly, the ^{87}Sr/^{86}Sr ratios significantly increase from the central portions (0.709–0.713, see Table 4) of the carbonate-rich rocks to the altered haloes (Fig. 5), thus, clearly suggesting that the carbonate rocks of the eastern Himalayan syntaxis were contaminated by the country rocks with high ^{87}Sr/^{86}Sr ratios. This is another feature pointing to formation of the carbonate-rich dykes of the eastern Himalayan syntaxis from melts.

Table 6
K–Ar ages of phlogopite from dolomitic dykes in the eastern Himalayan syntaxis

Sample	Weight (g)	K (%)	Ar (10^{-10}mol/g)	^{40}Ar (at.%)	^{40}Ar/^{40}K	Age (Ma)
Smaller dyke swarm	0.04220	6.05	58.1199	89.9	0.000322	5.5±0.2
Larger dyke swarm	0.06940	8.10	50.5825	84.9	0.000209	3.6±0.1

λ, 5.543×10^{-10}/year; Assuming ^{40}Ar/^{36}Ar, 295.5; ^{38}Ar diluent material made in Switzerland was utilized to dilute ^{40}Ar. Gas was cleaned through titanium sponge.

Table 7
Average and range of compositions for carbonate dykes as well as comparison with published values of mantle-derived carbonatites and sedimentary carbonates

	Calcitic dykes 1		Calciocarbonatites 2		Limestone 3	Dolomitic dykes 1		Magnesiocarbonatites 2		Dolomite 3
Wt%	Average	Range	Average	Range	Average	Average	Range	Average	Range	Average
SiO_2	11.3	7.26–13.9	2.72	0.0–8.93	6.00	5.57	0.06–11.2	3.63	0.6–9.40	7.85
TiO_2	0.14	0.09–0.21	0.15	0.0–1.09		0.05	0.01–0.08	0.33	0.0–1.98	
Al_2O_3	1.64	0.83–2.50	1.06	0.0–6.89	1.20	1.02	0.01–2.83	0.99	0.0–4.41	0.97
Fe_2O_3	0.10	0.07–0.15	2.25	0.0–9.28	0.35	0.05	0.01–0.09	2.41	0.0–9.57	0.38
FeO	1.09	0.86–1.29	1.01	0.0–4.70	0.32	0.66	0.25–1.33	3.93	0.0–10.4	0.55
MgO	2.86	2.47–3.18	1.8	0.0–8.11	6.53	21.8	18.2–23.1	15.1	9.25–24.8	16.6
CaO	47.4	46.5–49.0	49.1	39.2–55.4	42.8	30.9	29.2–35.5	30.1	20.8–47	30.4
Na_2O	0.22	0.20–0.25	0.29	0.0–1.73	0.10	0.10	0.07–0.14	0.29	0.0–2.23	0.09
K_2O	1.26	0.40–2.82	0.26	0.0–1.47	0.34	0.10	0.03–0.38	0.28	0.0–1.89	0.35
P_2O_5	0.07	0–0.16	2.1	0.0–10.4		0.02	0–0.08	1.9	0.0–11.3	
MnO	0.04	0.01–0.07	0.52	0.0–2.57		0.03	0.01–0.07	0.96	0.02–5.47	
F	n.d.		0.29	0.0–2.66		n.d.		0.31	0.03–2.10	
Cl	n.d.		0.08	0.0–0.45		n.d.		0.07		
SrO	XXX		0.86	0.0–3.29		XXX		0.69	0.06–1.50	
BaO	XXX		0.34	0.0–5.0		XXX		0.64	0.01–4.30	
SO_3	n.d.		0.88	0.02–3.87		n.d.		1.08	0.06–2.86	
Trace elements in ppm										
Sr	297	220–391	XXX		390	354	55.3–2629	XXX		122
Y	11.0	7.28–14.4	119	25–346	5.4	4.49	2.37–8.32	61	5–120	3.2
Zr	14.7	6.47–24.6	189	4–2320	16	16.6	0.54–41.3	165	0–550	14
Nb	2.90	1.47–4.69	1204	1–15,000	2	1.14	0.02–2.64	1422	10–16,780	2
Ba	170	4.7–241	XXX		52	70.5	2.16–313	XXX		81
La	12.2	7.11–18.5	608	90–1600	6.0	4.74	1.70–11.3	764	95–3655	4.5
Ce	21.7	13.9–31.1	1687	74–4152	11	8.92	2.81–24.5	2183	147–8905	8.6
Pr	2.56	1.63–3.73	219	50–389	1.3	1.01	0.39–2.61	560		1
Nd	9.38	6.43–13.32	883	190–1550	5.5	3.71	1.50–9.62	634	222–1755	4.2
Sm	1.93	1.31–2.65	130	95–164	1.04	0.79	0.39–1.78	45	33–75	0.8
Eu	0.42	0.32–0.60	39	29–48	0.22	0.18	0.07–0.33	12	3.0–20	0.18
Tb	0.30	0.20–0.40	9	9.0–10.0	0.15	0.12	0.05–0.27	4.5	0.9–8	0.12
Yb	0.93	0.74–1.13	5	1.5–12	0.45	0.37	0.13–0.86	9.5	1–52	0.35
Lu	0.14	0.11–0.16	0.7		0.07	0.05	0.02–0.12	0.08		0.055
Total REE	54.7	35.2–78.3	3731		28.2	21.9	7.81–55.8	4212		22.2
Th	4.08	2.48–5.70	52	5–168	1.1	1.34	0.02–4.12	93	4–315	0.9
U	1.56	0.56–3.47	8.7	0.3–29	1.3	0.48	0.02–2.01	13	1–42	0.87
Sc	2.73	2.03–3.40	7	0.6–18	1.4	0.75	0.06–2.38	14	10.0–17.0	1.1
V	10.7	0–20.7	80	0–300	13	11.95	8.23–21.4	89	7–280	11
Cr	8.76	1.91–14.7	13	2–479	8.3	0.71	0–2.70	55	2–175	5.6
Co	6.27	3.95–9.90	11	2.0–26	1.50	5.02	1.50–8.53	17	4–39	1.3
Ni	25.9	10.9–49.1	18	5.0–30	5	8.33	6.69–11.1	33	21–60	4.2
Cu	3.98	1.86–6.40	24	4–80	4.2	8.40	0–66.3	27	4–94	3.7
Zn	9.99	4.43–13.6	188	20–1120	19	11.4	0–55.5	251	15–851	15
Rb	19.0	12.9–23.8	14	4–35	10	2.89	0–9.45	31	2–80	8

n.d., not detected; (1) from Tables 3a and b; (2) from Woolley and Kempe (1989); (3) after Yan and Chi (1997). XXX gives either oxides in wt% or elements in ppm.

6.2. Melt origin in the mantle or in crustal levels?

The eastern Himalayan carbonatite-like dykes are markedly distinct to most known mantle-derived carbonatites (Table 7). Mineralogically, the carbonate rocks of the eastern Himalayan syntaxis do not contain pyrochlore series minerals, alkaline minerals and REE-bearing minerals typically occurring in mantle-derived carbonatites. In contrast to that, the carbonatite-like dykes show mineral assemblages similar to those of granulite-facies marbles. For example, the eastern Himalayan carbonatite-like dykes contain a B-bearing mineral, warwickite, which is common in metasedimentary rocks. Silicate minerals, such as olivine, spinel and phlogopite, can also be found in high-temperature marbles (Table 2). Compositionally, the carbonate rocks of the eastern Himalayan syntaxis are poor in most incompatible elements, such as REEs, U, Th, P, Sr and Ba. The alkaline contents are also relatively low

(Tables 3a and b) similar to some sedimentary carbonate rocks. Especially the carbon and radiogenic isotope signatures of the carbonatite-like dykes are similar to those of sedimentary limestones (e.g. Tuttle and Gittins, 1966; Javoy et al., 1986; Bell and Blenkinsop, 1989; Deines, 1989). From the above similarities to (meta)sedimentary limestones, the melts forming the carbonate dykes are compatible with melting of sedimentary limestones (e.g. Tuttle and Gittins, 1966).

Although carbonatites and associated alkali-ultramafic rocks found in Italy show signatures of high $^{87}Sr/^{86}Sr$, low $^{143}Nd/^{144}Nd$, and low REE contents (Castorina et al., 2000) very similar to those reported here, clear differences exist between the Italian and the Himalayan carbonate-rich rocks. The Italian carbonatites contain mantle xenoliths (Castorina et al., 2000) and have typical mantle $\delta^{13}C$ values close to $-2‰$ (Stoppa and Woolley, 1997), whereas the Himalayan rocks show typical $\delta^{13}C$ values ($>0‰$) of marine carbonates (Javoy et al., 1986) and contain xenoliths of granulite facies gneisses as mentioned above (Fig. 2a). In addition, no associated alkali ultramafic rocks that are commonly related to the Italian carbonatites were found around the eastern Himalayan carbonatite-like dykes. Thus, we favour the idea that the melts forming our rocks originated in crustal levels. This is also supported by experimental studies. Wyllie and Tuttle (1960) described that at a pressure of 1 kbar and in the presence of H_2O limestone begins to melt at 740 °C. Moreover, a mixture of small amounts of CO_2 in the H_2O-rich fluid could enhance limestone melting. Fanelli et al. (1986) added MgO to the $CaO–H_2O–CO_2$ system and observed that the eutectic temperature was even as low as about 600 °C. These results clearly indicate that carbonate magmas could be produced at crustal levels by melting of sedimentary carbonates. Considering the scapolite hornblendite associated with the dolomites that shows $\varepsilon Nd > 0$ (Table 4, Fig. 5), mantle or lower-crustal high-temperature fluids might have played a role in the melting of sedimentary carbonates as suggested above. Additionally, the involvement of 'juvenile' fluids is also supported by the oxygen isotope data of the calcitic dykes (Table 4, Fig. 5).

Structural analyses have shown that the carbonate dykes occur beneath or at the bottom of the Greater Himalayan Crystallines (Fig. 1a and b). Considering that the carbonate melts have low viscosities (perhaps the lowest of any terrestrial rock melts), low temperatures and low densities compared to silicate melts (see summery by Bell and Tilton, 2002), the remobilized carbonate melts could have even contributed to the exhumation of the Greater Himalayan Crystallines (GHC). This suggests that the Greater Himalayan Crystallines of the eastern Himalayan syntaxis exhumed during late Neogene based on the K–Ar and Ar–Ar geochronology data mentioned-above.

6.3. Petrogenetic model

The following petrogenetic model is presented considering the geochemical data of the eastern Himalayan carbonatite-like dykes and that melts forming these dykes have intruded the granulites of the Greater Himalayan Crystallines since the late Neogene. As well the hot Greater Himalayan Crystallines were exhumed from beneath south Tibet via ductile channel flow to overlie the limestone/marble-bearing upper Lesser Himalayan Crystallines southeastwards. Stacking of the hot Greater Himalayan Crystallines with fluids enriched in H_2O and poor in CO_2 probably from the lower crust or even mantle over the limestone/marble-bearing Lesser Himalayan Crystallines could have triggered the remobilization of the latter. Moreover, the melts reacted with the Greater Himalayan Crystallines to form rocks such as the scapolite hornblendite and to release CO_2. Such a process is similar to rock formation in skarn systems. According to the experiments (Wyllie and Tuttle, 1960; Fanelli et al., 1986), the released CO_2, adding to the H_2O-rich fluids, could have further lowered the melting temperature of limestone to form carbonate melts continually. The heat for the melting process might be also provided by the stacking of the hot Greater Himalayan Crystallines. The carbonate melts, in turn, could have played a role in regard of the exhumation of the Greater Himalayan Crystallines lately.

7. Conclusions

Carbonate dykes within the eastern Himalayan syntaxis occur along the contact between the Greater Himalayan Crystallines and the upper Lesser Himalayan Crystallines, or at the base of the Greater Himalayan Crystallines. Geochemical, isotopic, and petrological evidence has shown that these carbonate dykes resulted from remobilized (meta) sedimentary carbonate rocks triggered probably by the stacking of the Greater Himalayan Crystallines. In turn, the remobilized carbonate melts contributed to the exhumation of the latter, suggesting that the Greater Himalayan Crystallines rose to surface during late Neogene based on K–Ar and Ar–Ar data obtained on amphibole and mica from the carbonate dykes.

The investigated rocks provide a rare example for the origin of carbonate-rich dykes formed from melts that originated from sedimentary rocks.

Acknowledgements

We thank Weiguo Huo for guiding analyses of C and O isotopes, and Claudia Moessner, Xingdi Jin and Heping Zhu for assistance undertaking ICP-MS analyses. Thomas Theye and Ralf Schweinehage supported the electron microprobe

analyses at Universität Stuttgart. The beneficial comments or revisions on earlier versions of the manuscript by Yosuke Kawachi are gratefully acknowledged. Constructive reviews by A. Jones and D. Lentz significantly improved the manuscript. We also appreciated the criticism by Keith Bell. This work was supported by the Key National Basic Research Program Project of China (2002CB412601), Ministry of Land and Resources, China (No. 200101020405), the NSFC grants 49802018 and 40272044 and a DAAD scholarship.

Reference

Achterbergh, E.V., Griffin, W.L., Ryan, C.G., O'Reilly, S.Y., Pearson, N.J., Kivi, K., Doyle, B.J., 2002. Subduction signature for quenched carbonatites from the deep lithosphere. Geology 30, 743–746.

Al-Aasm, I.S., Taylor, B.E., South, B., 1990. Stable isotope analysis of multiple carbonate samples using selective acid extraction. Chemical Geology 80, 119–125.

Bailey, D.K., 1989. Carbonate melt from the mantle in the volcanoes of south-east Zambia. Nature 338, 414–418.

Barker, D.S., 1996. Consequences of recyled carbon in carbonatites. Canadian Mineralogist 34, 373–387.

Beaumont, C., Jamieson, R.A., Nguyen, M.H., Lee, B., 2001. Himalayan tectonics explained by extrusion of a low-viscosity crustal channel coupled to focused surface denudation. Nature 414, 738–742.

Bell, K., Blenkinsop, J., 1989. Neodymium and strontium isotope geochemistry of carbonatites, in: Bell, K. (Ed.), Carbonatites: Genesis and Evolution. Unwin Hyman, London, pp. 278–300.

Bell, K., Tilton, G.R., 2002. Probing the mantle: the story from carbonatites. Eos 83, 273–277.

Blum, J.D., Gazis, C.A., Jacobson, A.D., Chamberlain, C.P., 1998. Carbonate versus silicate weathering in the Raikhot watershed within the High Himalayan crystalline series. Geology 26, 411–414.

Boynton, W.V., 1984. Cosmochemistry of the rare earth elements: meteorite studies, in: Henderson, P. (Ed.), Rare Earth Element Geochemistry. Elsevier, Amsterdam, pp. 63–114.

Burg, J.-P., Nievergelt, P., Oberli, F., Seward, D., Davy, P., Maurin, J.-C., Diao, Z., Meier, M., 1998. The Namche-Barwa syntaxis: evidence for exhumation related to compressional crustal folding. Journal of Asian Earth Sciences 16, 239–252.

Castorina, F., Stoppa, F., Cundari, A., Barbieri, M., 2000. An enriched mantle source for Italy's melilitite-carbonatite association as inferred by its Nd-Sr isotope signature. Mineral Magazine 64, 625–639.

Deines, P., 1989. Stable isotope variations in carbonatites, in: Bell, K. (Ed.), Carbonatites: Genesis and Evolution. Unwin Hyman, London, pp. 301–359.

Droop, G.T.R., 1987. A general equation for estimating Fe^{3+} microprobe analyses, using stoichiometric criteria. Mineral Magazine 51, 431–435.

Evans, M.J., Derry, L.A., Anderson, S.P., France-Lanord, C., 2001. Hydrothermal source of radiogenic Sr to Himalayan rivers. Geology 29, 803–806.

Fanelli, M.T., Cava, N., Wyllie, P.J., 1986. Calcite and dolomite without portlandite at a new eutectic in CaO–MgO–CO_2–H_2O with applications to carbonatites. In: Morphology and Phase Equilibria of Minerals, Proceedings of the 13th General Meeting of the International Mineralogical Association, Bulgarian Academy of Science: Sofia, pp. 313–322.

Grujic, D., Casey, M., Davidson, C., Hollister, L., Kundig, R., Pavlis, T., Schmid, S., 1996. Ductile extrusion of the higher Himalayan crystalline in Bhutan: Evidence from quartz microfabrics. Tectonophysics 260, 21–43.

Grujic, D., Hollister, L., Parrish, R.R., 2002. Himalayan metamorphic sequence as an orogenic channel: Insight from Bhutan. Earth and Planetary Science Letters 198, 177–191.

Harmer, R.E., Lee, C.A., Eglington, B.M., 1998. A deep mantle source for carbonatite magmatism: evidence from the nephelinites and carbonatites of the Buhera district, SE Zimbabwe. Earth and Planetary Science Letters 158, 131–142.

Harris, N., Oliver, L., Bickle, M., Chapman, H., Dise, N., 2003. Silicate weathering rates decoupled from Sr-isotope ratios in the Himalaya. European Geophysical Society 2003 Geophysical Research Abstracts 5, 09019.

Hoernle, K., Tilton, G., Le Bas, M.J., Duggen, S., Garbe-Schongerg, C.D., 2002. Geochemistry of oceanic carbonatites compared with continental carbonatites: mantle recycling of oceanic crustal carbonate. Contributions to Mineralogy and Petrology 142, 520–542.

Javoy, M., Pineau, F., Delorme, H., 1986. Carbon and nitrogen isotopes in the mantle. Chemical Geology 57, 41–62.

Keller, J., Hoefs, J., 1995. Stable isotope characteristics of recent natrocarbonatites from Oldoinyo Lengai, In: Bell, K., Keller, J. (eds.), Carbonatite Volcanism: Lengai and Petrogenesis of Natrocarbonatites, IAVCEI Proceedings of Volcanology, IAVCEI, pp. 113–123.

Kjarsgaard, B.A., Hamilton, B.D., 1988. Liquid immiscibility and the origin of alkali-poor carbonatites. Mineral Magazine 52, 43–55.

Kretz, R., 1983. Symbols for rock-forming mineral. American Mineralogist 68, 277–279.

Krishnamurthy, P., Hoda, S.Q., Sinha, R.P., Banerjee, D.C., Dwivedy, K.K., 2000. Economic aspects of carbonatites of India. Journal of Asian Earth Sciences 18, 229–235.

Krishnaswami, S., Trivedi, J.R., Sarin, M.M., Ramesh, R., Sharma, K.K., 1992. Strontium isotopes and rubidium in the Ganga–Brahmaputra river system: weathering in the Himalaya, fluxes to the Bay of Bengal and contributions to the evolution of oceanic $^{87}Sr/^{86}Sr$. Earth and Planetary Science Letters 109, 243–253.

Le Bas, M.J., 1981. Carbonatite magmas. Mineral Magazine 44, 133–140.

Le Bas, M.J., 1987. Nephelinites and carbonatites, in: Fitton, J.G., Upton, B.G.J. (Eds.), Alkaline Igneous Rocks, vol. 30. Geological Society of London Special Publication, , pp. 85–94.

Le Bas, M.J., Keller, F., Tao, K., Wall, F., Williams, C.T., Zhang, P., 1992. Carbonatite dykes at Bayan Obo, Inner Mongolia, China. Mineralogy and Petrology 46, 195–228.

Le Bas, M.J., Subbarao, K.V., Walsh, J.N., 2002. Metacarbonatite or marble? The case of the carbonate, pyroxenite, calcite-apatite rock complex at Borra, Eastern Ghats, India. Journal of Asian Earth Sciences 20, 127–140.

Leake, B.E., Woolley, A.R., Birch, W.D., Gibert, M.C., Grice, J.D., Hawhtorne, F., Kato, A., Kisch, H.J., Krivovichev, V.G., Linthout, K., Laird, J., Mandarino, J.A., Maresch, W.V., Nickel, E.H., Rock, N.M.S., Schumacher, J.C., Smith, D.C., Srephenson, N.C.N., Ungaretti, L., Whittaker, E.J.W., Guo, Y.Z., 1997. Nomenclature of amphiboles: Report from the subcommittee on amphiboles of the International Mineralogical Association, commission on mew minerals and mineral names. American Mineralogist 82, 1019–1037.

Lentz, D.R., 1998. Late-tectonic U–Th–Mo–REE skarn and carbonatitic vein-dike systems in the southwestern Grenville Province: a pegmatite-related pneumatolytic model linked to marble melting (limestone syntexis), in: Lentz (Ed.), Mineralized Intrusion-Related Skarn Systems, vol. 26. Mineralogical Association of Canada Short Course, , pp. 519–657.

Lentz, D.R., 1999. Carbonatite genesis: a reexamination of the role of intrusion-related pneumatolytic skarn processes in limestone melting. Geology 27, 335–338.

Liu, Y., Zhong, D., 1997. Petrology of high-pressure granulite from the eastern Himalayan syntaxis. Journal of Metamorphic Geology 15, 451–466.

Liu, Y., Zhong, D., 1998. Tectonic framework of the eastern Himalayan syntaxis. Progress in Natural Science 8, 366–370.

Liu, G., Jin, C., Wang, F., Wang, S., Wang, B., Xu, R., Ding, X., 1990. Metamorphic and Igneous Rocks in Xizang (Tibet). People's Republic of China Ministry of Geology and Mineral Resources Geological Memoirs Series 3 No. 11. Geological Publishing House, Beijing p. 380, (in Chinese with English abstract).

Lombardo, B., Rolfo, F., 2000. Two contrasting eclogite types in the Himalayas: implications for the Himalayan orogeny. Journal of Geodynamics 30, 37–60.

Nelson, D.R., Chivas, A.R., Chappell, B.W., McCulloch, M.T., 1988. Geochemical and isotopic systematics in carbonatites and implications for the evolution of ocean-island sources. Geochemica et Cosmochimica Acta 52, 1–17.

Pognante, U., Benna, P., 1993. Metamorphic zonation, migmatization, and leucogranites along the Everest transect (Eastern Nepal and Tibet): record of an exhumation history, in: Treloar, P.J., Searle, M.P. (Eds.), Himalayan Tectonics, vol. 74. Geological Society of London, special publication, , pp. 323–340.

Searle, M.P., Simpson, R.L., Law, R.D., Parrish, R.R., Waters, D.J., 2003. The structural geometry, metamorphic and magmatic evolution of the Everest massif, High Himalaya of Nepal–South Tibet. Journal of Geological Society 160, 345–366.

Simonetti, A., Bell, K., 1994. Isotopic and geochemical investigation of the Chilwa island carbonatite complex, Malawi: evidence for a depleted mantle source region, liquid immiscibility, and open-system behavior. Journal of Petrology 35, 1597–1621.

Stoppa, F., Woolley, A.R., 1997. The Italian carbonatites: field occurrence, petrology and regional significance. Mineralogy and Petrology 19, 43–67.

Sun, S.S., McDonough, W.F., 1989. Chemical and isotopic systematics of oceanic basalts: implications for mantle composition and process, in: Saunders, A.D., Norry, M.J. (Eds.), Magmatism in Ocean Basins, vol. 42. Geological Society of London, Special Publication, , pp. 313–345.

Teertstra, D.K., Sherriff, B.L., 1997. Substitutional mechanisms, compositional trends and the end-member formulae of scapolite. Chemical Geology 136, 233–260.

Tuttle, O.F., Gittins, J., 1966. Carbonatites. Wiley, New York p. 591.

Woolley, A.R., 1982. A discussion of carbonatite evolution and nomenclature, and the generation of sodic and potassic fenites. Mineral Magazine 46, 13–17.

Woolley, A.R., Kempe, D.R.C., 1989. Carbonatites: nomenclature, average chemical compositions, and element distribution, in: Bell, K. (Ed.), Carbonatites: Genesis and Evolution. Unwin Hyman, London, pp. 1–14.

Wyllie, P.J., Tuttle, O.F., 1960. The system $CaO–CO_2–H_2O$ and the origin of carbonatites. Journal of Petrology 1, 1–46.

Wyllie, P.J., Baker, M.B., White, B.S., 1990. Experimental boundaries for the origin and evolution of carbonatites. Lithos 26, 3–19.

Yan, M., Chi, Q., 1997. The Chemical Compositions of Crust and Rocks in the Eastern Part of China. Bejing Science Press. P. 292.

Yin, J., Guo, S., 1978. Stratigraphy of the Mount Jolmo Lungma and its north slope. Scientia Sinica 21, 629–644.